Matter

CellPress
OPEN ACCESS

Article

Degradation and self-repairing in perovskite light-emitting diodes

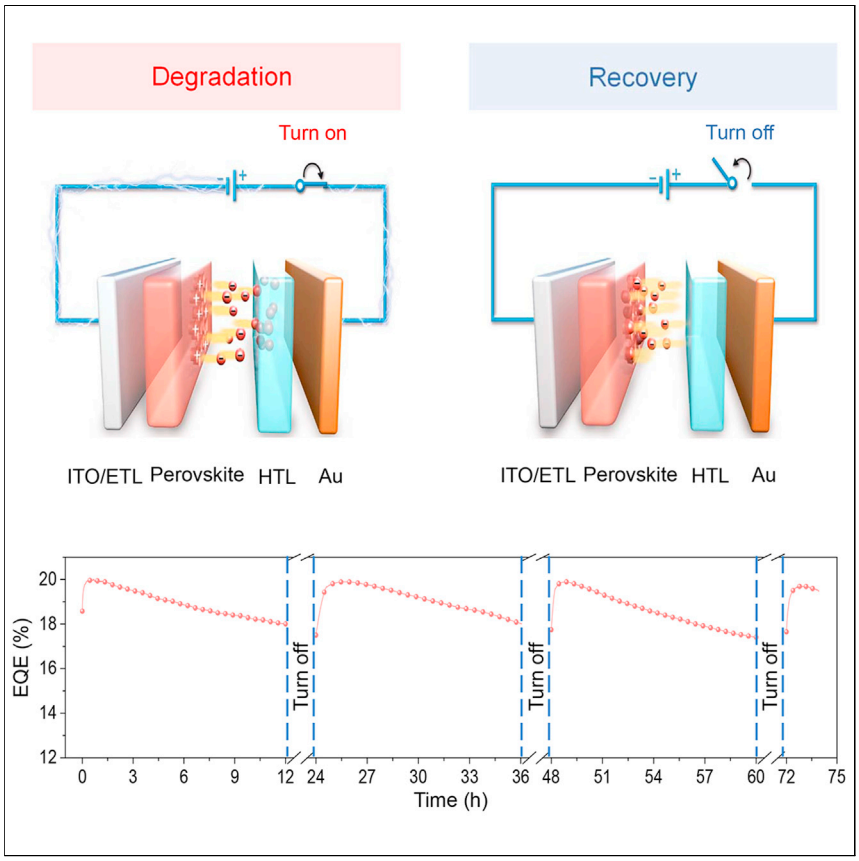

A key challenge that remains in perovskite light-emitting diodes is to achieve long-term operational stability. We find that the halide ions at perovskite surface migrate into the hole transport layer during operation, which works as one of the dominant device degradation pathways. Intriguingly, these ions can also gradually move back and consequently lead to the recovery of device performance. The repeatable performance recovery at room temperature can greatly help to enhance the long-term reliability of perovskite light-emitting devices in practical applications.

Pengpeng Teng, Sebastian Reichert, Weidong Xu, ..., Baoquan Sun, Carsten Deibel, Feng Gao

weidong.xu@liu.se (W.X.)
yingyang@nuaa.edu.cn (Y.Y.)
feng.gao@liu.se (F.G.)

Highlights

Moderately degraded devices can restore the performance after resting

Diffusion of halides from hole transport layer repairs perovskite surface defects

Critical role of perovskite/hole transport interface on the device stability

The self-repairing is attractive for long-term stability

1 Discovery
A new material or phenomena

Teng et al., Matter 4, 3710–3724
November 3, 2021
Published by Elsevier Inc.
https://doi.org/10.1016/j.matt.2021.09.007

CellPress
OPEN ACCESS

Matter

Article

Degradation and self-repairing in perovskite light-emitting diodes

Pengpeng Teng,[1,2,7,8] Sebastian Reichert,[3] Weidong Xu,[2,*] Shih-Chi Yang,[4] Fan Fu,[4] Yatao Zou,[5] Chunyang Yin,[2] Chunxiong Bao,[2] Max Karlsson,[2] Xianjie Liu,[6] Jiajun Qin,[2] Tao Yu,[8] Wolfgang Tress,[9] Ying Yang,[1,7,*] Baoquan Sun,[5] Carsten Deibel,[3] and Feng Gao[2,10,*]

SUMMARY

One of the most critical challenges in perovskite light-emitting diodes (PeLEDs) lies in poor operational stability. Although field-dependent ion migration is believed to play an important role in the operation of perovskite optoelectronic devices, a complete understanding of how it affects the stability of PeLEDs is still missing. Here, we report a unique self-repairing behavior that the electroluminescence of moderately degraded PeLEDs can almost completely restore to their initial performance after resting. We find that the accumulated halides within the hole transport layer undergo back-diffusion toward the surface of the perovskite layer during resting, repairing the vacancies and thus resulting in electroluminescence recovery. These findings indicate that one of the dominant degradation pathways in PeLEDs is the generation of halide vacancies at perovskite/hole transport layer interface during operation. We thus further passivate this key interface, which results in a high external quantum efficiency of 22.8% and obviously improved operational stability.

INTRODUCTION

Metal halide perovskite light-emitting diodes (PeLEDs) have achieved considerable progress during the last several years, with external quantum efficiencies (EQEs) rapidly exceeding 20%.[1–7] Despite recent advances in the efficiency, the reliability of PeLEDs remains a major obstacle, with operational lifetime as short as from several minutes to dozens of hours.[1,8,9] The poor stability of PeLEDs has been largely ascribed to Joule heating-induced material decomposition,[10–12] redox reaction between lead cations and diffusive Al^0,[13,14] as well as the environmental factors such as water or oxygen penetration.[15,16] In addition, based on previous investigations of perovskite solar cells, field-dependent ion migration and relevant material/interfacial degradation have been regarded as the most critical factors limiting the reliability of PeLEDs.[17–21] As such, there have been extensive efforts to improve the operational lifetime by immobilizing the ions, including perovskite composition engineering,[22] defect passivation, and construction of mixed-dimensional structures.[3,5,23–25] Nevertheless, a deep understanding of how ion-drifting influences PeLEDs' performance in detail remains missing, hindering targeted material design and device optimization for further improvement of the operational lifetime.

Here, we demonstrate that one of the dominant degradation pathways in state-of-the-art PeLEDs is the formation of halide vacancies at perovskite/hole transport layer (HTL) interface, resulting from field-dependent ion motion. This finding is firmly

Progress and potential

Despite the rapid improvement in efficiencies, achieving long-term reliable perovskite light-emitting diodes (PeLEDs) remains challenging, which impedes their practical applications. Further improvements in stability require a more fundamental understanding of the dominant degradation pathways in state-of-the-art PeLEDs. Here, we demonstrate that the halide vacancies generated at perovskite/hole transport interface during device operation are critical to electroluminescence quenching. This is on the basis of our deep understanding of an intriguing self-repairing phenomenon; that is, moderately degraded devices can almost completely restore to their initial performance after storage. We also note that this behavior is helpful to greatly enhance the reliability of PeLEDs in practical applications. Our findings provide a guideline for more targeted material and device optimization, highlighting the importance of the interface between the perovskites and hole transport layers.

based on our investigations on a unique self-repairing behavior in PeLEDs; that is, moderately degraded PeLEDs can almost completely recover to their initial performance after storage. Notably, the repeatable performance recovery at room temperature can help to enhance the long-term reliability of PeLEDs in practical applications, as the light-emitting diodes (LEDs) usually work intermittently rather than continuously. By performing a variety of characterizations, we establish the correlations between interfacial defect generation and field-dependent ion drift as well as between self-healing and ion back-diffusion, highlighting the importance of the interface between the perovskite and HTL on the device stability. We further passivate this critical interface and achieve PeLEDs with both high efficiency and much enhanced stability.

RESULTS AND DISCUSSION

Self-repairing in PeLEDs

Self-recovery of performance has been previously reported in perovskite photovoltaics, where the decreased short circuit current density caused by light irradiation can completely restore to the initial values after short-time storage (<1 min).[26] Similar behavior is also visible in perovskite single crystals where the photo-generated defects can be self-healed within several hours, leading to the recovery of photoluminescence (PL).[27] The mechanisms underlying these phenomena are still under debate. Theoretical calculations point out the key roles of small polarons and/or defect-trapped excitons.[26,28] Although self-recovery has been reported in photo-induced degradation, it has been rarely investigated in electrically driven PeLEDs.

We investigate two types of perovskite emitters: 2,2′-[oxybis(ethylenoxy)]diethylamine (ODEA)-passivated formamidinium (FA^+) lead tri-iodide ($FAPbI_3$) and $NMA_2FA_nPbI_{3n+1}$ perovskites with FA^+ as the cations and 1-naphthylmethylammonium iodide (NMAI) as the organic spacers.[5,6,29] The former are referred to as ODEA devices, and the latter are referred to as NMAI devices. These two PeLEDs represent two prevailing perovskite emitters based on three-dimensional (3D) and mixed-dimensional perovskites, respectively. We prepare PeLEDs with an architecture of indium tin oxide (ITO)/polyethylenimine ethoxylated: zinc oxide nanocrystals (ZnO:PEIE)/perovskite/poly(9,9-dioctyl-fluorene-co-N-(4-butylphenyl)diphenyl-amine) (TFB)/molybdenum oxide (MoO_3)/Au (Figure 1A). To avoid damage from solvent vapor residues in the glovebox to the PeLEDs, most of the devices discussed here were encapsulated and kept in clean N_2 atmosphere. The temperature in the glovebox is around 20°C–25°C. Unless otherwise stated, we use a large constant current density of 100 mA cm^{-2} to measure the maximum EQE values and accelerate device degradation, considering that it is among the largest values giving the peak performance as indicated by current density-EQE (J-EQE) characteristics (Figure S1). The half-operational lifetime (T_{50}) from batch to batch is typically within the range of 15–50 min for ODEA devices and 10–20 min for NMAI cases at 100 mA cm^{-2}.

After degradation, both types of device show self-recovery during the resting period (devices were turned off) in the glovebox at room temperature. As shown in Figures 1B and 1C, devices degraded to 50% of the initial values (day 0) display continuous EQE enhancements with prolonging the resting time, eventually leading to almost complete performance recovery (over 90% of its initial values) after 10 days. The characteristics of current density-voltage (J-V) curves are mostly preserved, and no shift of electroluminescence (EL) spectra is visible (Figure S1). In addition, we note that the self-recovery behavior is repeatable for the same device. In Figure 1D we show the self-recovery of a typical ODEA-device measured for three cycles. In

[1]State Key Laboratory of Mechanics and Control of Mechanical Structures, Nanjing University of Aeronautics and Astronautics, Nanjing 210016, China

[2]Department of Physics, Chemistry and Biology (IFM), Linköping University, Linköping 581 83, Sweden

[3]Institut für Physik, Technische Universität Chemnitz, Chemnitz 09126, Germany

[4]Laboratory for Thin Films and Photovoltaics, Empa–Swiss Federal Laboratories for Materials Science and Technology, Ueberlandstrasse 129, Duebendorf 8600, Switzerland

[5]Jiangsu Key Laboratory for Carbon-Based Functional Materials and Devices, Institute of Functional Nano and Soft Materials (FUNSOM), Joint International Research Laboratory of Carbon-Based Functional Materials and Devices, Soochow University, 199 Ren'ai Road, Suzhou, Jiangsu 215123, China

[6]Laboratory of Organic Electronics, Department of Science and Technology, Linköping University, Norrköping 60174, Sweden

[7]College of Materials Science and Technology, Nanjing University of Aeronautics and Astronautics, Nanjing 210016, China

[8]National Laboratory of Solid State Microstructures, Nanjing University, Nanjing 210093, China

[9]Institute of Computational Physics, Zurich University of Applied Sciences, Wildbachstr. 21, Winterthur 8401, Switzerland

[10]Lead contact

*Correspondence: weidong.xu@liu.se (W.X.), yingyang@nuaa.edu.cn (Y.Y.), feng.gao@liu.se (F.G.)

https://doi.org/10.1016/j.matt.2021.09.007

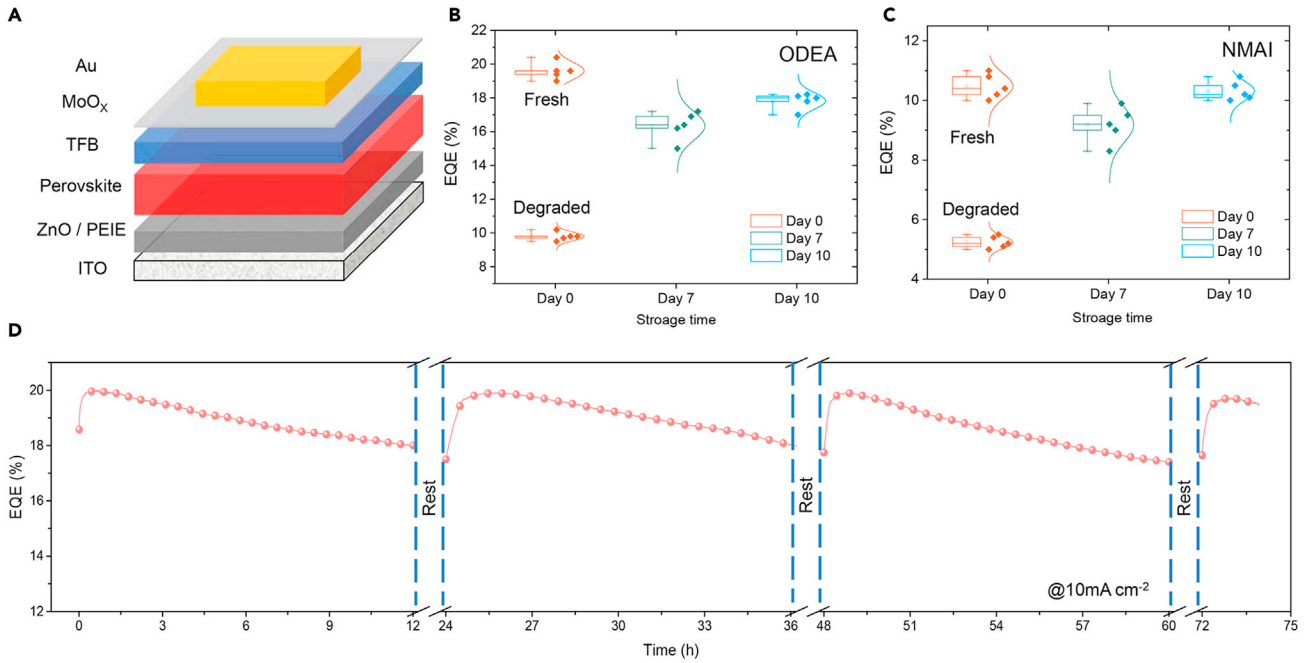

Figure 1. PeLEDs and recoverable EL

(A) A schematic diagram of the device structure.

(B and C) Peak EQE evolution of degraded ODEA (B) and NMAI (C) devices with storage time (measured at 100 mA cm^{-2}). The error bars represent the standard deviation extracted from five devices on the same ITO substrate. The boxes show the region containing 25%–75% of the data point; the lines and the squares in the boxes indicate the mean values and median values, respectively; the top and bottom lines out of the boxes suggest the maximum and minimum values, respectively; the curves denote the Gaussian distribution.

(D) Multi-cycles of device aging (measured at 10 mA cm^{-2}) and recovery at room temperature. Both aging and recovery procedures take 12 h in each cycle.

each cycle (24 h), the device is first operated at a constant current density of 10 mA cm^{-2} for 12 h, followed by resting for another 12 h. Encouragingly, the performance can be recovered to the initial value in all the cycles. The repeatable self-repairing is attractive for long-term reliability from the practical point of view, where the LEDs usually work intermittently rather than continuously.

To determine whether the self-recovery behavior arises from the intrinsic properties of perovskites, we perform a series of experiments to exclude the potential interfering factors in terms of atmosphere, perovskite compositions, and device structures.[30,31] We observe a similar performance recovery after resting the half-degraded devices in vacuum (Figure S2), excluding the possible effect from the atmosphere. We also fabricate PeLEDs with different device structures and perovskite compositions; that is, a p-i-n architecture of ITO/poly(9-vinylcarbazole) (PVK)/green emissive perovskite/2,2′,2"-(1,3,5-benzinetriyl)-tris(1-phenyl-1-H-benzimidazole) (TPBi)/Al. Here, the green emissive perovskite is a mixed-dimensional $CsPbBr_3$ with phenethylammonium bromide (PEABr) as the spacer layers.[32] As shown in Figure S3, the degraded devices also present performance recovery (from 65% of its initial EQE to 80% after resting), although it is not as significant as that in n-i-p devices. Previous reports have suggested that thermal diffusion of Al atoms toward the perovskite layer leads to the formation of Pb^0 due to the redox reaction.[13,14] The presence of an additional irreversible degradation pathway might be the reason that p-i-n devices show less significant performance recovery.

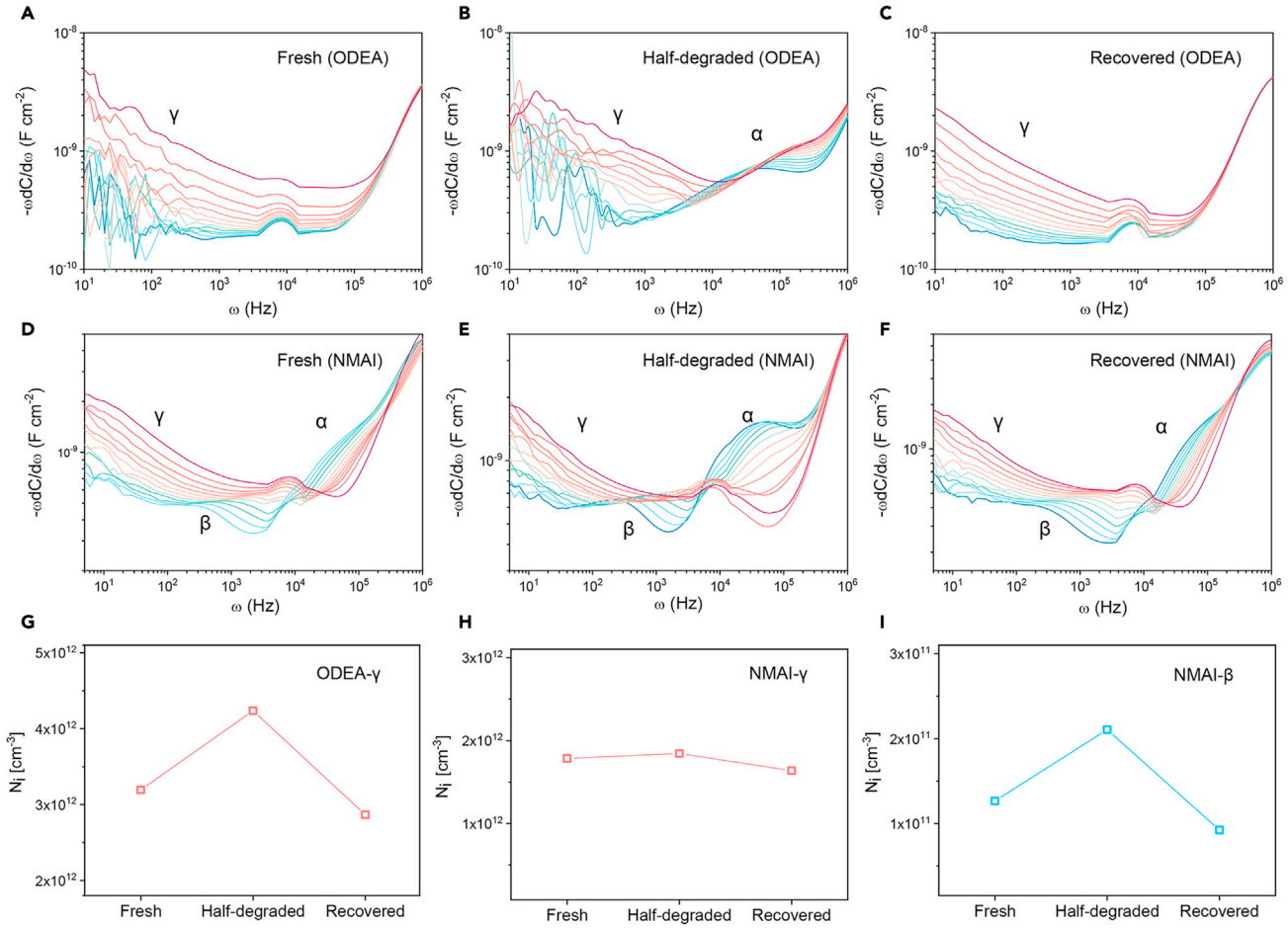

Figure 2. Defect physics in different types of devices

(A–F) Derivatives of temperature-dependent capacitance versus frequency plots for ODEA (A–C) and NMAI (D–F) devices. Here, fresh (A and D), half-degraded (B and E), and recovered devices (C and F) are characterized. The sets of capacitive response are labeled as γ, β, and α. The color changes from blue to red represent the temperature variations from 240 K to 300 K in 5 K increments. For all the tests an AC voltage with amplitude of 20 mV was applied.

(G–I) Mobile ion concentration (N_i) deduced by the TAS results: (G) γ in ODEA devices, (H) β and (I) γ in NMAI devices.

Characterizations of trap states and mobile ions

The decreases in device performance are generally associated with defect generation caused by material degradation under electrical bias. We thus perform thermal admittance spectroscopy (TAS) on fresh, half-degraded, and recovered devices. Both ODEA and NMAI devices are investigated. By varying the frequency (ω) of an applied alternating voltage at different temperatures, the capacitance (C) response of mobile ionic species and defects can be probed. It allows us to deduce the parameters of electronic defects in the high-frequency region and mobile ions in the low-frequency region.[33,34] We show the capacitance-frequency (C-f) characteristics in Figure S4 and the plots of derivatives (-ωdC/dω versus ω) in Figures 2A–2F. In brief, we observe the appearance of three sets of response peaks associated with different frequencies and temperatures in the fresh NMAI devices (Figure 2D), but only one in the fresh ODEA devices (Figure 2A). The sets of signatures are labeled γ, β, and α, which correspond to the slow capacitive responses at high temperatures, and moderate and fast responses at low temperatures, respectively, as shown in the Arrhenius plots (Figure S5).

Table 1. Parameters of the electronic defect α with activation energy E_A capture cross section σ and trap density N_t for half-degraded samples

Half-degraded devices	E_A [eV]	σ [cm^2]	N_t [cm^{-3}]
NMAI	0.24	9.5×10^{-18}	2.6×10^{15}
ODEA	0.25	1.3×10^{-17}	2.7×10^{15}

To distinguish the nature of capacitive responses in TAS results (that is, either from mobile ionic species or electronic defects), we perform deep-level transient spectroscopy (DLTS) with injection pulses from zero to forward bias and additionally with opposite pulse conditions (R-DLTS).[35,36] While the rate of ion drifting has little dependence on the pulse direction, the capture and emission rates of charge carriers trapped in electronic defects differ significantly. Given that fresh NMAI devices show all the three sets of responses (γ, β, and α), we studied them more closely. By varying the temperature, all the responses in NMAI devices were characterized (Figure S6) and assigned according to the Arrhenius plots (Figure S7). As shown in the boxcar evaluation of DLTS and R-DLTS (Figure S6), the responses for γ and β occur on comparable time scales in both DLTS and R-DLTS measurements. These results confirm that both originate from mobile ionic species, consistent with the TAS results that these responses emerge in the lower frequency region. In contrast, the capture rate of α in R-DLTS is one order of magnitude faster than the emission rate shown in DLTS, implying that the α responses in TAS arise from electronic defects.

Notably, the signatures of electronic states (α) are much more prominent in half-degraded NMAI devices and become discernible in ODEA cases (Figures 2B and 2E). Accordingly, we deduce the defect parameters of α including activation energy (E_A), capture cross section (σ), and trap density (N_t), which are summarized in Table 1. The low E_A values for both NMAI (~0.24 eV) and ODEA devices (~0.25 eV) indicate the shallow nature of these trap states. The σ and N_t values are $\sim 10^{-17}$ cm^2 and $\sim 10^{15}$ cm^{-3} for both cases, respectively, which are in a typical range as previously reported for hybrid perovskites.[37,38] In contrast, the α signals in recovered devices (Figures 2C and 2F) are as low as their respective fresh counterparts, and both are not distinct enough to give good signal to noise ratio and thus are hard to use to accurately determine reliable defect parameters. Nevertheless, these results clearly suggest that the generated electronic defect states in the degraded samples undergo self-healing after resting.

Having revealed the generation of defect sites and their self-healing, we proceed to analyze the parameters for mobile species (γ and β), including activation energy for ion migration (E_A'), ion diffusion coefficient at 300 K (D_{300K}), and concentration of mobile ions (N_i). In brief, we note that the E_A' values are very close in each set of devices (fresh, half-degraded, and recovered), and all the D_{300K} values are within the same order of magnitude, indicating that the mode of ion migration and the migration rates are not strongly changed. In addition, the N_i values for β of NMAI devices and γ of NMAI devices are slightly increased in both types of half-degraded devices compared with the fresh and recovered counterparts (Figures 2G–2I). These results indicate that the ion drifting becomes more prominent in the degraded devices, but remains more or less identical in fresh and recovered cases. Hence, this leads to more severe J-V hysteresis upon scan direction in half-degraded devices (Figure S8).[2,39] The slightly enhanced ion migration could be a result of newly formed defects that provide more hopping sites for ionic species.[40,41] All the detailed parameters for mobile ions are summarized in Table S1.

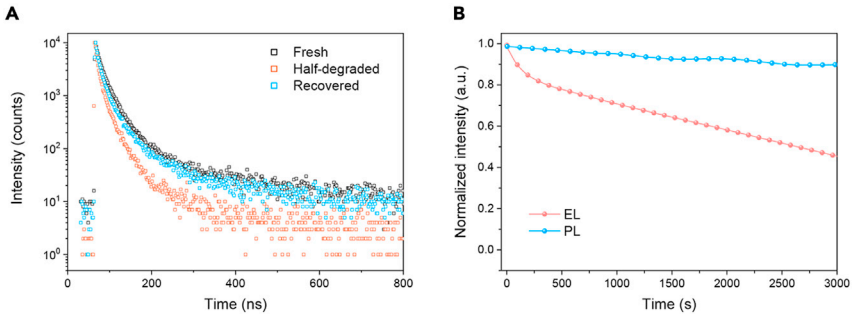

Figure 3. Characterization of trap states

(A) PL decay of various ODEA devices (fresh, half-degraded, recovered) measured by TCSPC.

(B) PL and EL intensities of ODEA devices versus the operational time.

Further evidence on the defect generation and their self-healing is obtained from time-correlated single photon counting (TCSPC) measurements, which are performed on completed ODEA devices as an example (with contacts) (Figure 3A). All these data are recorded from the same pixel. We note that the PL lifetime of perovskite layer becomes shorter after electric stressing (half-degraded) but turns to as long as that of the fresh case after resting. This further confirms the defect generation during operation and the following self-healing behavior. Additionally, we notice that occasionally half-degraded devices cannot show any signs of recovery after resting for a long time. In this case, we still observe the recovery of PL lifetime (Figure S9), suggesting that the self-defect repairing still occurs, but other factors, such as the degradation of organic charge transport layers, could represent an irreversible degradation mechanism hindering performance recovery.

To understand whether the generated defects concentrate at the surface or distribute across the entire perovskite layer, we simultaneously measure PL and EL on the devices by using chopped light (80 Hz) from continuous-wave laser (450 nm) and a lock-in amplifier. We find that the decrease in EL intensity is much more significant than PL (Figure 3B). Particularly, the half-degraded devices still preserve more than 90% of the initial PL intensity. As such, the defect generation during device operation is most likely to be concentrated at the interface of the perovskite layer.

Mechanisms behind self-healing of defects

We use various techniques to probe the structural evolution of perovskites within the devices, aiming to provide a rationale for the recoverable EL from the material point of view. We first perform time-of-flight secondary ion mass spectrometry (ToF-SIMS) depth profiling. NMAI devices are selected as the candidates because of their smooth film morphology, while the rugged surface of ODEA films is not desired for accurately determining the ion distribution in the direction perpendicular to the substrates (Figure S10). Figure 4A presents the ion distribution of fresh, half-degraded, recovered, and completely degraded devices. All these data were collected from different pixels on the same substrate. In the half-degraded samples, we observe increases in iodide signals within the TFB layer compared with the fresh ones. In addition, a much larger number of iodides are visible in the Au layer of the completely degraded cases. This owes much to field-dependent halide migration, in which negatively charged ions move toward the anode under positive electric bias. Notably, for the recovered samples, the distribution of iodide signals is almost identical to that in fresh counterparts, implying that the

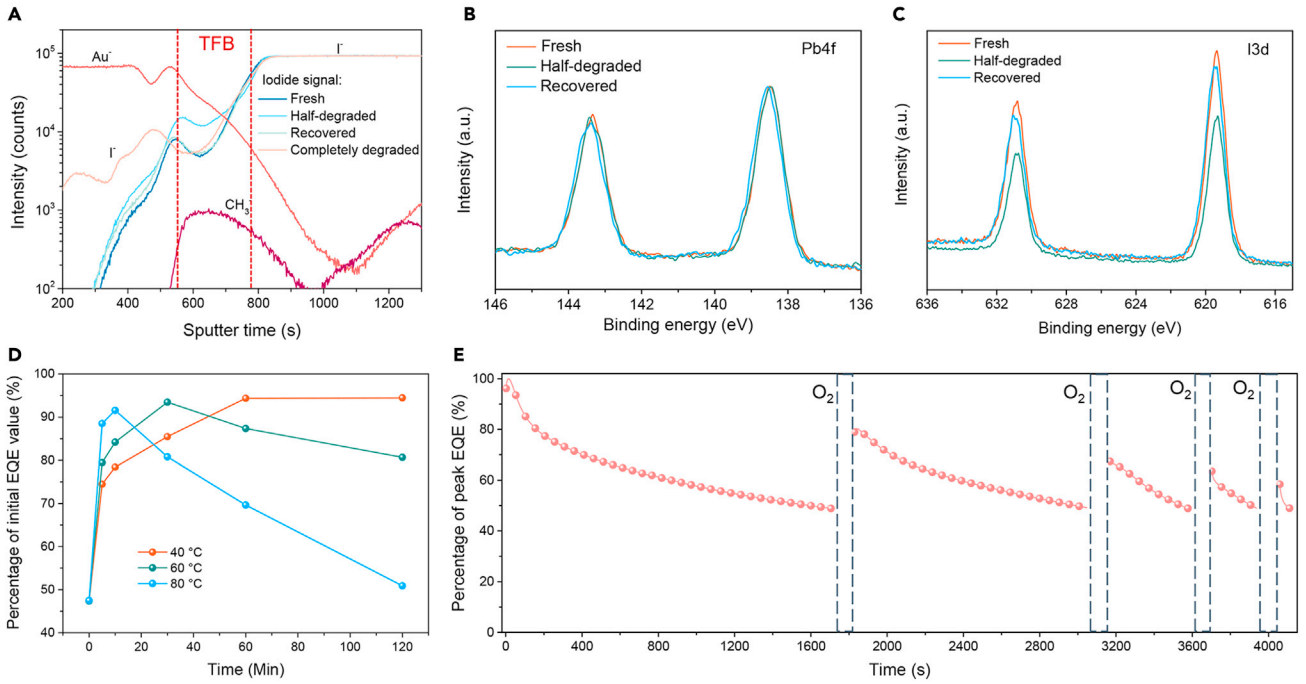

Figure 4. Disentangling the factors underlying the self-repairing of devices

(A–C) (A) ToF-SIMS depth profiling conducted on NMAI devices (fresh, half-degraded, recovered, and completely degraded), showing depth profiles of I^-, Au^-, and CH_3^- ions. Surface elemental characterizations on perovskite films of ODEA devices (fresh, half-degraded, recovered) by XPS tests: Pb 4*f* (B) and I 3*d* (C).

(D) Temperature-dependent dynamics for EL recovery.

(E) Multi-cycles of device aging and the effect of oxygen treatment.

accumulated iodides within the TFB layer can move back to the perovskite layer after resting.

Although the rugged surface of ODEA films makes it difficult to obtain reliable information of the ion distribution using the ToF-SIMS technique, our X-ray photoelectron spectroscopy (XPS) measurements on ODEA samples provide results consistent with the NMAI cases. The ODEA samples for XPS measurements, including fresh, half-degraded, and recovered cases, are prepared by chlorobenzene rinsing to remove the top contact layers. The core-level spectra of Pb and I are shown in Figures 4B and 4C, from which we calculate the elemental stoichiometric ratios for iodine referenced to Pb by integrating the respective peak area and with relative atomic sensitivity factors in consideration. The I/Pb ratios are 3.8, 2.6, and 3.7 for fresh, half-degraded, and recovered samples respectively. These results are in line with the ToF-SIMS results on the NMAI samples, suggesting that surface halide deficiency of the perovskite layer caused by field-dependent ion drifting, as well as their back-diffusion during the resting period, are the reasons for device degradation and self-repairing respectively.

Since halide back-diffusion is now demonstrated to be the underlying reason behind EL recovery, the recovery dynamics are supposed to rely on the temperature due to the thermodynamic nature of ion diffusion. Figure 4D shows the EQE evolution of the half-degraded devices at different temperatures. As expected, the required recovery time is significantly shortened at high temperatures. It takes ~3 min, ~30 min, and ~60 min for recovery of half-degraded devices to over 90% of initial EQEs at

80°C, 60°C, and 40°C, respectively. It is worth mentioning that a high temperature of over 60°C damages the devices, as shown by the fact that long duration of treatment decreases the device performance. In addition, a temperature as low as −18°C can freeze the recovery; in this case, no improvement can be observed after 10 days of storage (Figure S11). These observations are consistent with the dependence of ion diffusion coefficient on temperature, which further confirms that ion back-diffusion is crucial for EL recovery.

Another phenomenon that additionally supports the generation of halide vacancies and self-repairing being the main reasons behind device degradation and recovery is the remarkable oxygen passivation effect. We find that a very short-term (~2 min) exposure of degraded devices to dry oxygen atmosphere leads to dramatically enhanced peak EQE values. In contrast, no improvement is visible by resting the degraded devices in N_2 for the same duration (Figure S12). This is in good agreement with previous reports that negatively charged superoxide (O_2^-) can bond with halide vacancies (V_I^+), leading to an enhancement of the PL properties.[42,43] We notice that although oxygen-exposure-induced EL recovery can be performed cyclically, as shown in Figure 4E, the effects become less pronounced with increasing the number of cycles, possibly due to the fact that superoxide penetration into perovskites can also result in perovskite degradation.[16,44] In addition, as revealed in the previous report, oxygen passivation is a temporary effect that tends to gradually diminish in N_2 atmosphere due to oxygen desorption.[30] As such, the self-defect repairing caused by halide back-diffusion still occurs in oxygen-treated devices (Figure S13).

With all the collected evidence, we are now able to present the mechanisms for the dominant degradation pathway and EL recovery in PeLEDs, as illustrated in Figures 5A and 5B. In analogy to the other prevailing LEDs, luminance of a PeLED typically presents a double exponential decay including an initial fast component and a subsequent slow one.[1,45] Given that the half-degraded PeLEDs can at least recover to ~90% of their initial luminance, the fast decay component in the current cases is dominated by the field-dependent halide migration toward HTL at the surface of perovskite layer. The directional ion motion leads to the formation of a larger number of positively charged vacancies (V_I^+) distributed at the interface, leading to severe EL quenching (Figure 5A). Once the bias is removed, the halides within the HTL undergo directional back drifting to the surface of perovskites, repairing the defects and thus recovering the EL (Figure 5B). Notably, this is an uphill diffusion process in which halides move toward the region with high ion concentration.[45] We thus believe that this process is driven and manipulated by the electrostatic potential gradients due to the presence of a reversed electric field caused by space charges. This takes over the effect of concentration gradients and pushes the negatively charged ions to move back and heal the vacancies. The dynamics of device recovery is consistent with the proposed model, as the recovery speed slows down over time as a result of decreased potential gradients (Figure S14). Since ion diffusion is a thermally activated process as well, a high temperature can reduce or overcome the energy barrier and hence facilitate halide back-diffusion, while a low temperature can mitigate or even freeze the recovery. The diffusion dynamics may be described by the Nernst-Planck equation, but more systematic modeling work is required.[46] Anyway, our findings suggest that the self-repairing in PeLEDs is fundamentally different from the previously observed self-recovery of PL from photo-induced damage.

Although the back-diffusion of halide anions and relevant self-recovery of the EL can contribute to the long-term stability of PeLEDs during practical applications, we

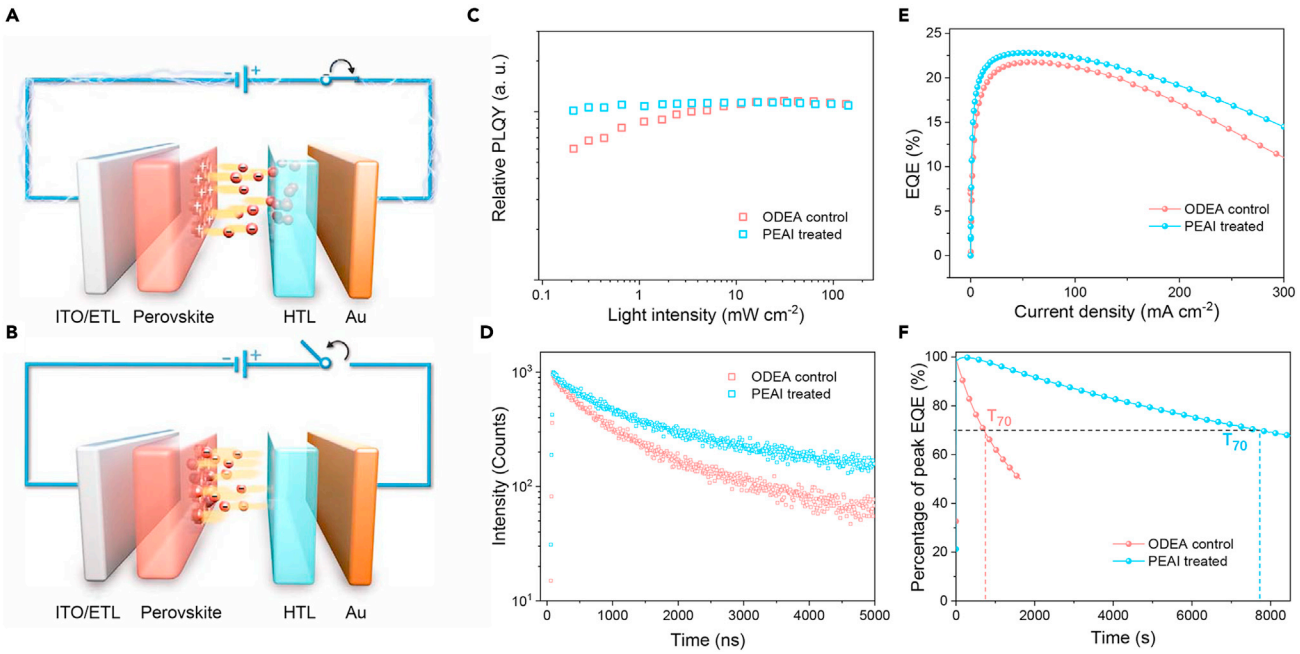

Figure 5. The mechanisms and a remedying solution to improve the stability

(A and B) The degradation and recovery process of PeLEDs. Defect generation due to halide drift under the electrical bias (A); defect self-repairing due to electrostatic potential-driven halide diffusion toward perovskite layer (B).

(C–F) Photophysics and the key device characteristics for ODEA-perovskites with and without post-PEAI treatment. Relative PLQYs dependent on excitation fluence (C); PL decay probed by TCSPC (D); EQE-current density (EQE-J) curves (E); operational lifetime at a constant current density of 100 mA cm^{-2} (F).

highlight that it is more critical to suppress the halide migration in the first place. Based on the mechanisms revealed above, surface engineering strategies including surface passivation or introducing a block layer between HTL and perovskites would be very promising to boost the operational stability. We thus treat this key interface by 2-phenethylammonium iodide (PEAI) solutions.[47,48] To identify the functionality of PEAI treatment in the current case, we measure relative photoluminescence quantum yields (PLQYs) as a function of excitation fluence, as well as PL lifetime by TCSPC tests, of which the results are shown in Figure 5C and 5D respectively. Compared with that of ODEA-control samples, the PLQYs of PEAI-treated thin films are much higher at low excitations (below ~3 mW cm^{-2}) and almost independent upon excitation fluence ranging from ~0.2 to ~140 mW cm^{-2}. In addition, a prolonged PL lifetime is achieved. Although the peak value of PLQY remains unchanged, these results are clearly suggestive of further elimination of defect sites by this post surface treatment.

As expected, the defect management at the perovskite/HTL interface brings about a much-prolonged device operational lifetime; i.e., a T_{70} (70% of its initial EQE value) of ~7,700 s at a current density of 100 mA cm^{-2} (with initial radiance ~110 W sr^{-1} m^{-2}) compared with ~700 s of ODEA-control films (with initial radiance ~100 W sr^{-1} m^{-2}) (Figure 5E). We also note that the PEAI post treatment leads to slight increases in the peak EQEs/maximum radiance (Figures 5F and S15). Particularly, a high EQE of 22.8% has been achieved, which is among the best so far for near-infrared (NIR) PeLEDs.

In summary, we have revealed a unique self-repairing behavior in PeLEDs where the performance of moderately degraded devices can restore to over 90% of its initial value after resting. This phenomenon arises from the back-diffusion of halides (driven by electrostatic potential) within the HTL toward the interface of perovskite, a process that repairs the halide vacancies at the interface and results in the self-annihilation of trap states. In this regard, we demonstrate that one of the dominant degradation pathways in state-of-the-art PeLEDs is the generation of halide vacancies at the perovskite/HTL interface caused by field-dependent ion drifting during operation. We have validated our findings by passivating the defects between perovskite and HTL, resulting in significantly prolonged operational lifetime. Our findings indicate the critical role of interfacial damage on the device stability and pave the way for stable PeLEDs by rational interfacial engineering.

EXPERIMENTAL PROCEDURES

Resource availability

Lead contact

Feng Gao, e-mail (feng.gao@liu.se).

Materials availability

This study did not generate new unique materials.

Data and code availability

The data presented in this work are available from the lead contact upon reasonable request.

Device fabrication and characterization

The details for fabricating ODEA passivated $FAPbI_3$ devices and NMAI-based mixed-dimensional perovskites ($NMA_2FA_nPbI_{3n+1}$) have been described in the previous literature.[5,6,29] In detail, 0.13 mmol of PbI_2, 0.26 mmol of formamidinium iodide (FAI), and 0.039 mmol of ODEA were mixed and dissolved in 1 mL of dimethylformamide (DMF) to prepare the ODEA precursor solution. In addition, 0.12 mmol of PbI_2, 0.12 mmol of FAI, and 0.12 mmol of NMAI were mixed in 1 mL of DMF for preparing the NMAI precursor. In addition, the precursor solutions for green PeLEDs were prepared by mixing 0.2 mmol of $PbBr_2$, 0.2 mmol of CsBr, 0.08 mmol of phenethylammonium bromide (PEABr), and 4.0 mg of 1,4,7,10,13,16-hexaoxacyclooctadecane (18-crown-6) in 1 mL of dimethyl sulfoxide (DMSO). The ZnO nanocrystals were synthesized according to the literature.[5]

ITO glass substrates were subsequently cleaned with deionized water and ethanol, followed by UV-ozone treatment for 20 min before use. For ODEA and NMAI devices, ZnO nanoparticles were spin coated on the cleaned ITO substrates at 4,000 rpm for 30 s in ambient conditions. Afterward, the coated substrates were moved into a N_2-filled glovebox for the deposition of PEIE (1.1 mg mL^{-1} in isopropanol). The perovskite layer was deposited at a spin-casting rate of 3,000 rpm. The thickness of NMAI films is around 50 nm. Due to the nano-island feature, it is hard to accurately determine the thickness of ODEA films. Both as-casted ODEA and NMAI films were annealed at 100°C for 10 min. For the surface passivation, 2-phenethylammonium iodide (0.25 mg mL^{-1} in isopropanol) was dynamically spin-coated on the annealed perovskite films at 3,000 rpm for 30 s and annealed at 100°C for 3 min. TFB (12 mg mL^{-1} in chlorobenzene) was then spin-coated on top of the perovskite films at 3,000 rpm for 30 s. The thickness of TFB is around 50 nm on NMAI films. After that, the substrates were moved into a thermal evaporator for the deposition of MoO_3 (7 nm) and Au (80 nm) layers. For green PeLEDs, poly(9-

vinylcarbazole) (PVK) solution (average Mn = 25,000–50,000, 6 mg mL^{-1} in chlorobenzene, ~10 nm) was spin coated on the cleaned ITO substrate at 3,000 rpm for 40 s in the glovebox, followed by thermal annealing at 120°C for 20 min. Afterward, the perovskite solution was deposited at a spin-cast rate of 3,000 rpm. The perovskite films were annealed at 100°C for 1 min. Finally, TPBi (40 nm) and electrode of LiF (1 nm)/Al (100 nm) were deposited by the thermal evaporator. The active area of our PeLEDs is 7.25 mm^2.

All the PeLEDs were measured with a Keithley 2400 source meter incorporated with a QE Pro spectrometer (Ocean Optics) at room temperature in a N_2-filled glovebox. The absolute radiance value was calibrated by a visible-NIR light source (HL-3P-INT-CAL plus, Ocean Optics). The ODEA and NMAI devices were operated at a constant current density of 50 mA cm^{-2} to determine peak EQE values. A large current density of 100 mA cm^{-2} was used to accelerate device degradation. For J-V characteristics, the devices were swept from zero bias to forward bias with one step of 0.05 V and for 300 ms each step. The active area of our devices is 7.25 mm^2.

Thin-film characterization

TCSPC for PL lifetime was measured by using an Edinburgh Instruments spectrometer (FLS1000) with a 635-nm picosecond laser (less than 100 ps, 1 MHz for complete ODEA devices, and 0.2 MHz for the ODEA- and PEAI-treated perovskite thin films). The instrument response function (IRF) is less than 200 ps. To accurately evaluate the evolution of PL decay after degradation and recovery, all the data are collected from different pixels on the same substrate. The relative PLQY is performed by using a 450-nm continuous-wave laser and calculated as the integrated PL intensity divided by the excitation fluence.[49] The thicknesses of charge transport layer and NMAI films in the devices are determined by a Dektak profile system. The morphology of perovskite films was measured by a scanning electron microscope (SEM; LEO 1550 Gemini).

XPS measurements were conducted by using a Scienta ESCA 200 spectrometer in ultrahigh vacuum (~1×10^{-10} mbar). A monochromatic Al (Kα) X-ray source was used to provide photons with 1,486.6 eV. The full width at half-maximum of the clean Au $4f_{7/2}$ line (at the binding energy of 84.00 eV) was 0.65 eV. All the spectra were recorded at a photoelectron take-off angle of 90°. The thin-film samples for XPS measurements were obtained from rinsing complete devices with chlorobenzene to remove the contacts and TFB layer. The XPS measurements were performed within 12 h once the devices were degraded. The X-ray beam was set to focus on each pixel of the same substrate.

In situ EL and PL measurements

The degradation of PL and EL of PeLEDs with encapsulation were measured simultaneously in ambient conditions at room temperature. A square function wave voltage (80 Hz) from a function generator (Tektronix AFG 3000) was used to drive the excitation light (450-nm laser diode). A Keithley 2400 source meter was used to test PeLEDs at a constant current of 100 mA cm^{-2}. An optical power detector (Newport, 818-UV/DB) was used to detect PL and EL signals, and the excitation light was filtered by a long-pass filter. The photocurrent signals (including the modulated PL and DC EL signals) of the optical power detector were first amplified using a low-noise current preamplifier (Stanford Research System, SR570) and measured using a lock-in amplifier (modulated PL signal) and a source meter (DC EL signal). The intensity of PL was controlled to less than 1/100 of the EL intensity by adjusting the driving voltage amplitude of the laser diode.

ToF-SIMS

ToF-SIMS measurements were performed on a ToF-SIMS.5 instrument (IONTOF, Germany) operated in spectral mode using a 25 keV Bi^{3+} primary ion beam with an ion current of 0.5 pA. For depth profiling, a 500 eV Cs^{+} sputter beam with a current of 20 nA was used to remove the material layer by layer in interlaced mode from a raster area of 300 × 300 μm. Negative ions were collected for depth profile analysis. The mass spectrometry was performed on an area of 50 × 50 μm in the center of the sputter crater. ToF-SIMS measurements were performed on two different batches of NMAI devices and the results are consistent.

TAS and DLTS

TAS and DLTS were performed with a Zurich Instrument MFLI lock-in amplifier with impedance analyzer (MF-IA) and multi-demodulator (MF-MD) options. The temperature of the samples was controlled by a cryo probe station Janis ST500 with a Lakeshore 336 temperature controller from 240 to 300 K in 5-K steps with accuracy of 0.01 K using liquid nitrogen. For all measurements, an alternating current (AC) voltage with amplitude of 20 mV was applied. The defect characterizations with TAS are according to the previous literature.[34] In brief, the emission rates (e_t) are obtained from the peak maxima of the derivative of the capacitance. These rates are linked to either diffusion coefficient D (Equation 1) or capture cross section (σ) (Equation 2):

$$e_t = \frac{e^2 N_{\text{eff}} D}{k_B T \varepsilon_0 \varepsilon_R} \qquad \text{(Equation 1)}$$

$$e_t = \sigma \overline{v_n} N_C \exp\left(-\frac{E_A}{k_B T}\right), \qquad \text{(Equation 2)}$$

where N_{eff} refers to the effective doping density, e is the elementary charge, k_B is the Boltzmann constant, T the temperature, ε_0 the dielectric constant, ε_R the relative permittivity, $\overline{v_n}$ the thermal velocity of charge carriers, and N_C the effective density of states in the conduction band. The capture cross section can be determined from Equation 2 using the following relationships for $\overline{v_n}$ and N_C:

$$\overline{v_n} = \sqrt{\frac{8 k_B T}{\pi m_e^*}} \qquad \text{(Equation 3)}$$

$$N_c = \left[\frac{2\pi m_e^* k_B T}{h^2}\right]^{\frac{3}{2}} \qquad \text{(Equation 4)}$$

with the electron effective mass $m_e^* \approx m_e$ and h the Planck constant. The diffusion coefficient depends on the temperature:

$$D = D_0 exp\left(-\frac{E_A{}'}{k_B T}\right), \qquad \text{(Equation 5)}$$

where $E_A{}'$ is activation energy for ion migration and D_0 is the diffusion coefficient at infinite temperatures. $E_A{}'$ and D_0 are extracted from the slope and the cross section with the emission rate axis using Equations 1 and 5. By taking into account the surface polarization caused by the accumulation of mobile ions at the interfaces of the perovskite layer, the concentration of mobile ions N_i is determined as:

$$N_i = \frac{k_B T \Delta C^2}{e^2 \varepsilon_0 \varepsilon_R}. \qquad \text{(Equation 6)}$$

Here, ΔC refers to the capacitance step in the admittance spectra of the contributing ions. The trap density N_t was calculated by

$$N_t(E_\omega) = -\frac{V_{bi}}{eWk_BT}\omega\frac{dC}{d\omega} \quad \text{(Equation 7)}$$

$$E_\omega = k_BT\ln\left(\frac{2\sigma\overline{v_n}N_c}{\omega}\right). \quad \text{(Equation 8)}$$

For DLTS measurements, a frequency of 80 kHz was used and the pulse voltage was provided by a Keysight Technologies 33600A function generator. Different pulse voltage and temperatures were applied in order to measure all observed defects in DLTS and R-DLTS separately. The duration of the pulses was 50 ms. For half-degraded samples, the TAS and DLTS measurements were carried out immediately once the bias was removed. All tests were finished within 12 h.

SUPPLEMENTAL INFORMATION

Supplemental information can be found online at https://doi.org/10.1016/j.matt.2021.09.007.

ACKNOWLEDGMENTS

The authors thank Yuwei Guo, Prof. Ni Zhao, and Prof. Jianpu Wang for valuable discussions. We acknowledge the support from the ERC Starting Grant (no. 717026), the Swedish Energy Agency Energimyndigheten (no. 48758-1), and the Swedish Government Strategic Research Area in Materials Science on Functional Materials at Linköping University (Faculty Grant SFO-Mat-LiU no. 2009-00971). S.R. and C.D. thank the DFG for their support within the framework of SPP 2196 project (no. 424216076). P.T. is grateful for financial support from China Scholarship Council (no. 201906830040), the Nanjing University of Aeronautics and Astronautics PhD short-term visiting scholar project (grant no. 180608DF06), and the Priority Academic Program Development of Jiangsu Higher Education Institutions. F.F. acknowledges the funding from the Swiss Federal Office of Energy (SFOE)-BFE (project no. SI/501805-01). F.G. is a Wallenberg Academy Fellow.

AUTHOR CONTRIBUTIONS

F.G. and W.X. conceived the idea and supervised the project. W.X. and P.T. performed the experiments and analyzed the data. S.R. performed TAS and DLTS measurements, and analyzed the data under the supervision of C.D. S.Y. and F.F. performed TOF-SIMS measurements and analyzed the data. C.Y. performed PLQY tests and analyzed the data. X.L. performed XPS tests. Y.Z. prepared green LEDs under supervision of B.S.; Y.Y. and T.Y. supervised P.T. W.X., P.T., and F.G. wrote the manuscript. W.T., J.Q., C.B., and M.K. contributed to data analysis and provided revisions to the manuscript. All authors discussed the results and commented on the manuscript.

DECLARATION OF INTERESTS

The authors declare no competing interests.

Received: March 30, 2021
Revised: May 28, 2021
Accepted: September 3, 2021
Published: September 27, 2021

REFERENCES

1. Liu, X.K., Xu, W., Bai, S., Jin, Y., Wang, J., Friend, R.H., and Gao, F. (2021). Metal halide perovskites for light-emitting diodes. Nat. Mater. *20*, 10–21.
2. Tan, Z.K., Moghaddam, R.S., Lai, M.L., Docampo, P., Higler, R., Deschler, F., Price, M., Sadhanala, A., Pazos, L.M., Credgington, D., et al. (2014). Bright light-emitting diodes based on organometal halide perovskite. Nat. Nanotechnol. *9*, 687–692.
3. Cao, Y., Wang, N., Tian, H., Guo, J., Wei, Y., Chen, H., Miao, Y., Zou, W., Pan, K., He, Y., et al. (2018). Perovskite light-emitting diodes based on spontaneously formed submicrometre-scale structures. Nature *562*, 249–253.
4. Lin, K., Xing, J., Quan, L.N., de Arquer, F.P.G., Gong, X., Lu, J., Xie, L., Zhao, W., Zhang, D., Yan, C., et al. (2018). Perovskite light-emitting diodes with external quantum efficiency exceeding 20 per cent. Nature *562*, 245–248.
5. Xu, W., Hu, Q., Bai, S., Bao, C., Miao, Y., Yuan, Z., Borzda, T., Barker, A.J., Tyukalova, E., Hu, Z., et al. (2019). Rational molecular passivation for high-performance perovskite light-emitting diodes. Nat. Photon. *13*, 418–424.
6. Zou, Y., Teng, P., Xu, W., Zheng, G., Lin, W., Yin, J., Kobera, L., Abbrent, S., Li, X., Steele, J.A., et al. (2021). Manipulating crystallization dynamics through chelating molecules for bright perovskite emitters. Nat. Commun. *12*, 4831.
7. Stranks, S.D., and Snaith, H.J. (2015). Metal-halide perovskites for photovoltaic and light-emitting devices. Nat. Nanotechnol. *10*, 391–402.
8. Lu, M., Zhang, Y., Wang, S., Guo, J., Yu, W.W., and Rogach, A.L. (2019). Metal halide perovskite light-emitting devices: promising technology for next-generation displays. Adv. Funct. Mater. *29*, 1902008.
9. Quan, L.N., Rand, B.P., Friend, R.H., Mhaisalkar, S.G., Lee, T.W., and Sargent, E.H. (2019). Perovskites for next-generation optical sources. Chem. Rev. *119*, 7444–7477.
10. Zhao, L., Roh, K., Kacmoli, S., Al Kurdi, K., Jhulki, S., Barlow, S., Marder, S.R., Gmachl, C., and Rand, B.P. (2020). Thermal management enables bright and stable perovskite light-emitting diodes. Adv. Mater. *32*, 2000752.
11. Prakasam, V., Tordera, D., Bolink, H.J., and Gelinck, G. (2019). Degradation mechanisms in organic lead halide perovskite light-emitting diodes. Adv. Opt. Mater. *7*, 1900902.
12. Warby, J.H., Wenger, B., Ramadan, A.J., Oliver, R.D.J., Sansom, H.C., Marshall, A.R., and Snaith, H.J. (2020). Revealing factors influencing the operational stability of perovskite light-emitting diodes. ACS Nano *14*, 8855–8865.
13. Zhao, L., Kerner, R.A., Xiao, Z., Lin, Y.L., Lee, K.M., Schwartz, J., and Rand, B.P. (2016). Redox chemistry dominates the degradation and decomposition of metal halide perovskite optoelectronic devices. ACS Energy Lett. *1*, 595–602.
14. Zou, Y., Wu, T., Fu, F., Bai, S., Cai, L., Yuan, Z., Li, Y., Li, R., Xu, W., Song, T., et al. (2020). Thermal-induced interface degradation in perovskite light-emitting diodes. J. Mater. Chem. C *8*, 15079–15085.
15. Yang, R., Zhang, L., Cao, Y., Miao, Y., Ke, Y., Wei, Y., Guo, Q., Wang, Y., Rong, Z., Wang, N., et al. (2017). Inhomogeneous degradation in metal halide perovskites. Appl. Phys. Lett. *111*, 073302.
16. He, J., Fang, W.H., Long, R., and Prezhdo, O.V. (2019). Superoxide/peroxide chemistry extends charge carriers' lifetime but undermines chemical stability of $CH_3NH_3PbI_3$ exposed to oxygen: time-domain ab initio analysis. J. Am. Chem. Soc. *141*, 5798–5807.
17. Yuan, Y., and Huang, J. (2016). Ion migration in organometal trihalide perovskite and its impact on photovoltaic efficiency and stability. Acc. Chem. Res. *49*, 286–293.
18. Guo, Y., Jia, Y., Li, N., Chen, M., Hu, S., Liu, C., and Zhao, N. (2020). Degradation mechanism of perovskite light-emitting diodes: an in situ investigation via electroabsorption spectroscopy and device modelling. Adv. Funct. Mater. *30*, 1910464.
19. Cheng, T., Tumen-Ulzii, G., Klotz, D., Watanabe, S., Matsushima, T., and Adachi, C. (2020). Ion migration-induced degradation and efficiency roll-off in quasi-2D perovskite light-emitting diodes. ACS Appl. Mater. Inter. *12*, 33004–33013.
20. Guerrero, A., You, J., Aranda, C., Kang, Y.S., Garcia-Belmonte, G., Zhou, H., Bisquert, J., and Yang, Y. (2016). Interfacial degradation of planar lead halide perovskite solar cells. ACS Nano *10*, 218–224.
21. Karlsson, M., Yi, Z., Reichert, S., Luo, X., Lin, W., Zhang, Z., Bao, C., Zhang, R., Bai, S., Zheng, G., et al. (2021). Mixed halide perovskites for spectrally stable and high-efficiency blue light-emitting diodes. Nat. Commun. *12*, 361.
22. Li, N., Song, L., Jia, Y., Dong, Y., Xie, F., Wang, L., Tao, S., and Zhao, N. (2020). Stabilizing perovskite light-emitting diodes by incorporation of binary alkali cations. Adv. Mater. *32*, 1907786.
23. Wang, H., Kosasih, F.U., Yu, H., Zheng, G., Zhang, J., Pozina, G., Liu, Y., Bao, C., Hu, Z., Liu, X., et al. (2020). Perovskite-molecule composite thin films for efficient and stable light-emitting diodes. Nat. Commun. *11*, 891.
24. Li, C., Wang, N., Guerrero, A., Zhong, Y., Long, H., Miao, Y., Bisquert, J., Wang, J., and Huettner, S. (2019). Understanding the improvement in the stability of a self-assembled multiple-quantum well perovskite light-emitting diode. J. Phys. Chem. Lett. *10*, 6857–6864.
25. Shang, Y., Liao, Y., Wei, Q., Wang, Z., Xiang, B., Ke, Y., Liu, W., and Ning, Z. (2019). Highly stable hybrid perovskite light-emitting diodes based on Dion-Jacobson structure. Sci. Adv. *5*, eaaw8072.
26. Nie, W., Blancon, J.C., Neukirch, A.J., Appavoo, K., Tsai, H., Chhowalla, M., Alam, M.A., Sfeir, M.Y., Katan, C., Even, J., et al. (2016). Light-activated photocurrent degradation and self-healing in perovskite solar cells. Nat. Commun. *7*, 11574.
27. Ceratti, D.R., Rakita, Y., Cremonesi, L., Tenne, R., Kalchenko, V., Elbaum, M., Oron, D., Potenza, M.A.C., Hodes, G., and Cahen, D. (2018). Self-healing inside $APbBr_3$ halide perovskite crystals. Adv. Mater. *30*, 1706273.
28. Nan, G., Zhang, X., and Lu, G. (2019). Self-healing of photocurrent degradation in perovskite solar cells: the role of defect-trapped excitons. J. Phys. Chem. Lett. *10*, 7774–7780.
29. Zou, W., Li, R., Zhang, S., Liu, Y., Wang, N., Cao, Y., Miao, Y., Xu, M., Guo, Q., Di, D., et al. (2018). Minimising efficiency roll-off in high-brightness perovskite light-emitting diodes. Nat. Commun. *9*, 608.
30. Galisteo-Lopez, J.F., Anaya, M., Calvo, M.E., and Miguez, H. (2015). Environmental effects on the photophysics of organic-inorganic halide perovskites. J. Phys. Chem. Lett. *6*, 2200–2205.
31. Alberti, A., Deretzis, I., Mannino, G., Smecca, E., Giannazzo, F., Listorti, A., Colella, S., Masi, S., and Magna, A. (2019). Nitrogen soaking promotes lattice recovery in polycrystalline hybrid perovskites. Adv. Energy Mater. *9*, 1803450.
32. Ban, M., Zou, Y., Rivett, J.P.H., Yang, Y., Thomas, T.H., Tan, Y., Song, T., Gao, X., Credgington, D., Deschler, F., et al. (2018). Solution-processed perovskite light emitting diodes with efficiency exceeding 15% through additive-controlled nanostructure tailoring. Nat. Commun. *9*, 3892.
33. Awni, R.A., Song, Z., Chen, C., Li, C., Wang, C., Razooqi, M.A., Chen, L., Wang, X., Ellingson, R.J., Li, J.V., et al. (2020). Influence of charge transport layers on capacitance measured in halide perovskite solar cells. Joule *4*, 644–657.
34. Reichert, S., An, Q., Woo, Y.W., Walsh, A., Vaynzof, Y., and Deibel, C. (2020). Probing the ionic defect landscape in halide perovskite solar cells. Nat. Commun. *11*, 6098.
35. Reichert, S., Flemming, J., An, Q., Vaynzof, Y., Pietschmann, J.-F., and Deibel, C. (2020). Ionic-defect distribution revealed by improved evaluation of deep-level transient spectroscopy on perovskite solar cells. Phys. Rev. Appl. *13*, 034018.
36. Futscher, M.H., Lee, J.M., McGovern, L., Muscarella, L.A., Wang, T., Haider, M.I., Fakharuddin, A., Schmidt-Mende, L., and Ehrler, B. (2019). Quantification of ion migration in $CH_3NH_3PbI_3$ perovskite solar cells by transient capacitance measurements. Mater. Horiz. *6*, 1497–1503.
37. Agiorgousis, M.L., Sun, Y.Y., Zeng, H., and Zhang, S. (2014). Strong covalency-induced recombination centers in perovskite solar cell material $CH_3NH_3PbI_3$. J. Am. Chem. Soc. *136*, 14570–14575.
38. Musiienko, A., Moravec, P., Grill, R., Praus, P., Vasylchenko, I., Pekarek, J., Tisdale, J., Ridzonova, K., Belas, E., Landová, L., et al. (2019). Deep levels, charge transport and

mixed conductivity in organometallic halide perovskites. Energy Environ. Sci. *12*, 1413–1425.

39. Wang, H., Chen, Z., Hu, J., Yu, H., Kuang, C., Qin, J., Liu, X., Lu, Y., Fahlman, M., Hou, L., et al. (2021). Dynamic redistribution of mobile ions in perovskite light-emitting diodes. Adv. Funct. Mater. *31*, 2007569.

40. Barker, A.J., Sadhanala, A., Deschler, F., Gandini, M., Senanayak, S.P., Pearce, P.M., Mosconi, E., Pearson, A.J., Wu, Y., Srimath Kandada, A.R., et al. (2017). Defect-assisted photoinduced halide segregation in mixed-halide perovskite thin films. ACS Energy Lett. *2*, 1416–1424.

41. Shao, Y., Fang, Y., Li, T., Wang, Q., Dong, Q., Deng, Y., Yuan, Y., Wei, H., Wang, M., Gruverman, A., et al. (2016). Grain boundary dominated ion migration in polycrystalline organic–inorganic halide perovskite films. Energy Environ. Sci. *9*, 1752–1759.

42. Liu, S.C., Li, Z., Yang, Y., Wang, X., Chen, Y.X., Xue, D.J., and Hu, J.S. (2019). Investigation of oxygen passivation for high-performance all-inorganic perovskite solar cells. J. Am. Chem. Soc. *141*, 18075–18082.

43. Motti, S.G., Gandini, M., Barker, A.J., Ball, J.M., Srimath Kandada, A.R., and Petrozza, A. (2016). Photoinduced emissive trap states in lead halide perovskite semiconductors. ACS Energy Lett. *1*, 726–730.

44. Aristidou, N., Eames, C., Sanchez-Molina, I., Bu, X., Kosco, J., Islam, M.S., and Haque, S.A. (2017). Fast oxygen diffusion and iodide defects mediate oxygen-induced degradation of perovskite solar cells. Nat. Commun. *8*, 15218.

45. Féry, C., Racine, B., Vaufrey, D., Doyeux, H., and Cinà, S. (2005). Physical mechanism responsible for the stretched exponential decay behavior of aging organic light-emitting diodes. Appl. Phys. Lett. *87*, 213502.

46. Krishna, R. (2015). Uphill diffusion in multicomponent mixtures. Chem. Soc. Rev. *44*, 2812–2836.

47. Guo, Y., Apergi, S., Li, N., Chen, M., Yin, C., Yuan, Z., Gao, F., Xie, F., Brocks, G., Tao, S., et al. (2021). Phenylalkylammonium passivation enables perovskite light emitting diodes with record high-radiance operational lifetime: the chain length matters. Nat. Commun. *12*, 644.

48. Jiang, Q., Zhao, Y., Zhang, X., Yang, X., Chen, Y., Chu, Z., Ye, Q., Li, X., Yin, Z., and You, J. (2019). Surface passivation of perovskite film for efficient solar cells. Nat. Photon. *13*, 460–466.

49. Motti, S.G., Meggiolaro, D., Barker, A.J., Mosconi, E., Perini, C.A.R., Ball, J.M., Gandini, M., Kim, M., Angelis, F.D., and Petrozza, A. (2019). Controlling competing photochemical reactions stabilizes perovskite solar cells. Nat. Photon. *13*, 532–539.